www.czasopisma.pan.pl PAN www.journals.pan.pl

jet INTL JOURNAL OF ELECTRONICS AND TELECOMMUNICATIONS, 2023, VOL. 69, NO. 2, PP. 239-245
Manuscript received October 25, 2022; revised April, 2023. DOI: 10.24425/ijet.2023.144356

A Dual-Band Compact Integrated Rectenna for Implantable Medical Devices

Shamil H. Hussein, and Khalid K. Mohammed

***Abstract*—This work describes a dual band compact fully integrated rectenna circuit for implantable medical devices (IMDs). The implantable rectenna circuit consists of tunnel diode 10×10µm^2 QW-ASPAT (Quantum Well Asymmetric Spacer Tunnel Layer diode) was used as the RF-DC rectifier due to its temperature insensitivity and nonlinearity compared with conventional SBD diode. SILVACO atlas software is used to design and simulate 100µm^2 QW InGaAs ASPAT diode. A miniaturized dual band implantable folded dipole antenna with multiple L-shaped conducting sections is designed using CST microwave suits for operation in the WMTS band is 1.5GHz and ISM band of 5.8GHz. High dielectric constant material Gallium Arsenide (ε_r=12.94) and folded geometry helps to design compact antennas with a small footprint of 2.84mm^3 (1×4.5×0.63) mm^3. Four-layer human tissue model was used, where the antenna was implanted in the skin model at depth of 2mm. The 10-dB impedance bandwidth of the proposed compact antenna at 1.5GHz and 5.8GHz are 227MHz (1.4-1.63GHz) with S_{11} is -22.6dB and 540MHz (5.47-6.02GHz) with S_{11} is -23.1dB, whereas gains are -36.9dBi, and -24.3dBi, respectively. The output DC voltage and power of the rectenna using two stage voltage doubler rectifier (VDR) are twice that produced by the single stage at input RF power of 10dBm.**

***Keywords*—Implantable rectenna; Folded Dipole Antenna FDA; Phantom tissues layers; CST suit; Simulation**

I. INTRODUCTION

IN recent years, growing global demand for clean renewable energy is a vital issue with major economic and social implications for our planet's future [1]. Therefore, the energy harvesting has become very important to collect energy from surrounding environments. Energy harvesting sources may be captured from the ambient environment or external [2]. Ambient energy is the process by which energy is derived from external sources [3], such as solar energy [4], wind energy [5], thermal energy [6], vibration-sourced piezoelectric [7], and electromagnetic ambient signals which involves radio-frequency RF energy [8], near electromagnetic field [9], and far-field electromagnetic signals [10]. The constant source of energy harvesting is the sun that captures rays by using solar cells. The cells represent the green energy that protects the environment from pollution. But the limitations of solar cells are little efficiency. Therefore, there are other solar inverter alternatives, such as radio frequency (RF) energy harvesting [11]. The main focus of this paper is on using miniaturized implantable rectenna for energy harvesting applications which used to capture environmental RF signals and convert them to DC voltage to drive low-power biomedical electronic devices such as implantable medical devices (IMDs) [12], wireless sensor networks [13], wireless energy harvesting [14], and wireless power transmission (WPT) [15].

The IMD devices have recently attracted the attention of scientists due to people are increasingly using these devices such as pacemakers [16], pill cameras [17], artificial arms, and measure human blood pressure and sugar in real time [18] as a result of recent advancements in the health-care system and specially after COVID 19 occurrence. Wireless charging is required for IMD devices that are implanted in the human body.

There are several challenges in the development of biomedical devices IMDs, which have been studied in depth in recent years with RF energy harvesting. As a result, this article focuses on antenna design and characterization in the presence of the human body, as well as introducing new antenna designs that handle some of the existing challenges, such as miniaturization, efficiency, frequency detuning, Patient safety and phantom tissues, Biocompatible, and integration. Also, In order to improve the performance of the implant antenna inside human tissue, It should be taken into consideration the interaction between embedded antennas and biological tissues which represent electrical permittivity (ε) and electrical conductivity (σ) [19]. Several structures of the implantable antennas design can be used to get miniaturization process such as serpentines [20], and spiral structure [21] is developed by Le Trong in 2021 [22] by using an open-ended slot at the ground for human head-implantable wireless communications utilizing a triple band antenna. Meander structure is reported in [23] and developed by Nikta in 2021 [24], fractal geometries [25], Flower-shape radiating patch [26], Circular Maze shaped [27], and several geometries shaped radiator are suggested in [28][29][30] for energy harvesting applications. The materials with a high ε of substrate, loading, and resonance frequency are techniques used to achieve miniaturization.

This paper presents; a compact dual band implantable planar dipole antenna design for medical applications with a small footprint of 2.835mm^3 (1×4.5×0.63) mm^3 and the 1µm thickness of the patch folded geometry. The proposed L-section planar dipole antenna operated at WMTS 1.5GHz for transmission of data (biotelemetry), and ISM 5.8GHz band which can wireless power transfer to drive IMDs devices. CST microwave studio was chosen to design and simulate the antenna. The simulated 10-dB impedance bandwidths in a four tissue layer phantom at 1.5GHz and 5.8GHz are 227MHz (1.4-1.63GHz) with S_{11} is -22.6dB and 540MHz (5.47-6.02GHz) with S_{11} is -23.1dB, whereas gains are -36.9dBi, and -24.3dBi, respectively. This

First author is with Faculty of Engineering University of Mosul, Iraq (e-mail: shamil_alnajjar84@uomosul.edu.iq).

Second author is with Faculty of Engineering University of Mosul and University of Nineveh, Iraq (e-mail: khalid.khaleel@uomosul.edu.iq).

implant FDA antenna can be integrated with QW-ASAPT rectifier diode to be used as an implantable rectenna circuit.

II. IMPLANTABLE ANTENNA DESIGN

Computer Simulation Technology (CST) microwave studio is used for the antenna design process [31]. Fig. 1. shows the basic model of the implant L-shaped planar dipole. All the optimized parameters are marked in Fig. 1 and detailed in table I. The antenna consists of two symmetrical radiating arms connected to a 50Ω feed discrete port. Each dipole arm flexes elaborately in a folding pattern that helps reduce the physical length of the antenna. Unlike typical folded dipoles, the developed antenna is not designed as a closed loop. We chose an open ended instead, as it offers great freedom to modify the antenna impedance and miniaturization capabilities. The FDA is implanted on the phantom consisting of four layers. The radiating planar structure is mounted on a high-permittivity dielectric substrate (Gallium arsenide, ε_r=12.94, tanδ=0.006) of 0.63mm thick semi-insulating GaAs substrate (h_s) and covered with an identical glue (h_{glue}) and superstrate (h_{super}) layer. Considering now antenna implantation into human arm skin, we employ a 4-layered tissue model consisting of skin, fat, muscle, and bone. The antenna is placed 2mm beneath the skin–air interface with its long axis parallel to it. Taking into account fabrication issues including glue layer (ε_r=3.5) of thickness 0.05 mm, superstrate layer of 0.63mm thick, gold metallization cladding 0.001mm and port feeding. The feed slot width (F) remained 0.1mm. In addition, a non-uniform metal strip widths of the main and secondary arm (w and t) were used along the antenna structure varying from 0.01 to 0.07mm in order to enhance effective antenna dimensions.

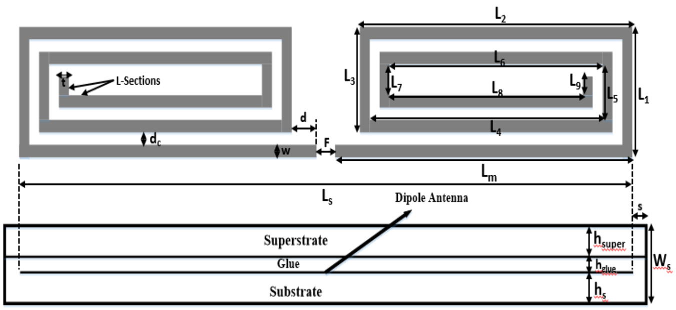

Fig. 1. Geometry of the 1×4.5mm^2 implantable FDA antenna structure with main and secondary L-section arms

TABLE I
OPTIMIZED DIMENTIONS OF THE PROPOSED ANTENNA

Parameter	Value [mm]	Parameter	Value [mm]
L_s	4.5	L_8	1.825
W_s	1	L_9	0.3
L_m	2.15	F	0.1
L_1	0.9	s	0.05
L_2	2.125	d	0.075
L_3	0.8	d_c	0.05
L_4	2.025	w = t	0.05
L_5	0.7	$h_s = h_{super}$	0.63
L_6	1.925	h_{glue}	0.05
L_7	0.9	h_c	0.001

The antenna structure consisted of a main conductive strip element and multiple L-shaped loading sections (strip-line width t = 0.05 mm) in each dipole arm, as shown in Fig. 1 and described in Table I. The four cases of L-type loaded antenna models are considered, respectively. All cases are designed to resonate at 1.5GHz and 5.8GHz with constant aperture width of (W_s=1 mm) and variable aperture length (L_s) depending on the number of applied L-sections. Feeding gap length (F) is kept constant throughout the analysis. Conductor spacing (d_c) and substrate gap (s) also remain stable. Furthermore, in each antenna model, the geometrical value regulating dipole arms coupling is optimized until the magnitude of the reflection coefficient (S_{11}) is below -15dB at the proposed dual bands. Performance characteristics such as antenna input impedance (Z_{Ant}), 10-dB impedance bandwidth (BW), and radiation efficiency (η_{rad}) corresponding to the cases examined are listed in table II.

TABLE II
PERFORMANCE CHARACTRISTICS OF THE PROPOSED ANTENNA WHEN OPERATION IN DUAL BANDS 1.5GHz AND 5.8GHz

Antenna Size [mm^2]	No. of L-section / Trace length [mm]	S_{11} [dB] 1.5GHz 5.8GHz	Gain [dBi] @ 1.5GHz @ 5.8GHz	B.W [MHz] @ 1.5GHz @ 5.8GHz	η_{rad} [%] @ 1.5GHz @ 5.8GHz	Z_{Ant} [Ω] @ 1.5GHz @ 5.8GHz
1 × 3	8 / 28	-29 -32	-39 -25.3	218 495	0.01 0.15	48+j*3.6 51+j*0.15
1 × 4.5 Proposed	4.5 / 26	-22.6 -23.1	-36.91 -24.3	227 540	0.013 0.17	58+j*2 57+j*2.4
1 × 7	3 / 29	-12 -21	-34.4 -24.7	255 570	0.021 0.182	86+j*1.2 60-j*0.4
1 × 9	2.5 / 32	-11 -13	-33.8 -24.5	290 590	0.023 0.2	91-j*0.57 77-j*8.6

Of note, it is observed from table II. The numerical results show that as the resonant dipole length decreases, the radiation efficiency degrades substantially. The (1×4.5) mm^2 antenna with 4.5 L-shaped sections has a minimum total trace length about 26.7mm which achieves size reduction of the proposed antenna dimensions in this work and explained in Fig. 1. Size reduction by 5% (eight L-type case), 8% (three L-type case), and 17% (2.5 L shaped section) relative to the 4.5 L-type configuration reduces radiation efficiency by 23%, 38%, and 44%, respectively. It is worth noting that the trace length for the 4.5 L-section case is 26.7 mm, while a simple straight dipole antenna is about 55 mm long is estimated by Eq. (1), both resonating at 5.8 GHz. The proposed planar loaded model is in fact a significantly shorter length (51% drop in physical length) relative to the straight configuration.

$$L_s = \frac{c}{2 * f * \sqrt{\varepsilon_{eff}}} \quad \text{……….. (1)}$$

Where L_s is the effective length of the folded dipole radiator, c is the speed of light, ε_{eff} is the effective dielectric constant of the substrate materials, and f is the operating frequency. Also, of note, the Z_{Ant} was extracted at proposed dual operating frequency. The 1×4.5mm^2 antenna has an Z_{Ant} at proposed bands are (58+j*2) Ω and (57+j*2.4) Ω respectively. The dependency of Z_{Ant} on the frequency provides a capacitive or inductive response at different frequencies. In this work, the antenna behaves inductively. It is observed that a 1×9mm^2 antenna with 2.5 L-shaped section operating at dual band has a η_{rad} of 0.023% and 0.2%. The gain of the proposed implant antenna is very low about -36.91dB and -24.3dB for dual bands, with a severely decreased η_{rad} of 0.013% and 0.17%, as a result of the antenna's reduction in size to 4.5mm^2. In general, tradeoffs between tiny size, reasonable gain, and radiation efficiency are required when the dipole geometry forms [32][33].

III. FURTHER OPTIMIZATION AND DISCUSSION

To check the mechanism of operation and improve the performance of the implanted antenna, some parameters are further analyzed.

A. Variations in the main and secondary arm width (w and t)

The effects of the both dimension main and secondary (w, and t) respectively of the antenna's arm width on the real part and imaginary part of our antenna impedance and reflection coefficients S_{11}. It has been found that changes in the width (w) significantly affect the real part of the Z_{Ant} (R_{Ant}) as shown in Fig. 2. while having a negligible effect on the imaginary part (jX_{Ant}). Similarly, the reactive value of the Z_{Ant} is greatly influenced by the width (t), allowing for the independent optimization of the R_{Ant} and jX_{Ant} of the folded antenna. The peak of R_{Ant} drops from high value of impedance nearly 600Ω to about 200Ω at w of 10μm and 70μm respectively when operating at the frequency of 2.45GHz, attributed to the smaller resistance associated with wider antenna arms. This was done while maintaining the width (t) at 50μm for operation at the proposed dual bands, thus the effect of each parameter is examined separately. Then, the effect of width (t) to antenna impedance has been taken with the width (w) is constant. Fig. 3 shows the effect of (t) on the imaginary part. It is clear from this figure that the effect (t) to the jX_{Ant} is greatly influenced.

According to Fig. 4, to make the S_{11} less than -15dB in the desired resonant dual band, the dimensions (w, t) of the antenna are selected as 50μm. It is observed that the effect widths to S_{11} at the frequency 5.8GHz is greatly influenced. The S_{11} is shifted to lower or higher than the frequency 5.8GHz.

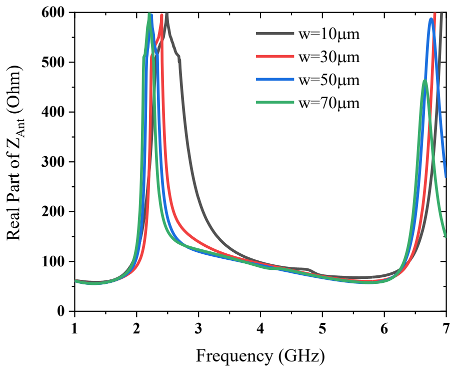

Fig. 2. Effects of the main arm dimension (w) on real part of Z_{Ant}

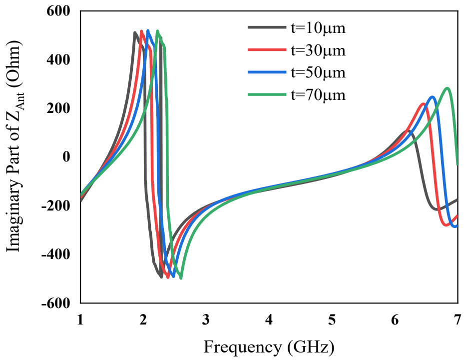

Fig. 3. Effects of the secondary arm dimension (t) on imaginary part of Z_{Ant}

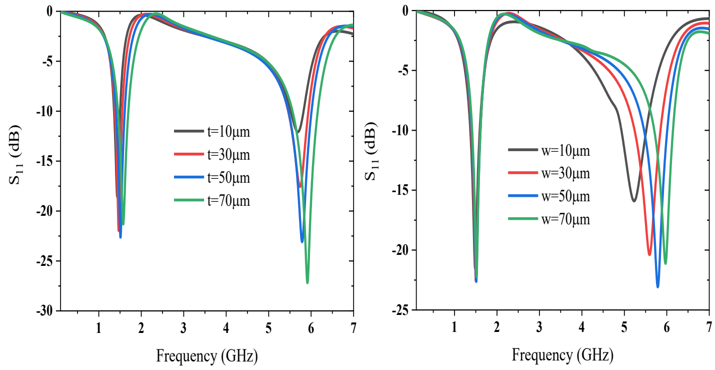

Fig. 4. Effects of the main and secondary arm dimension (w and t) on the proposed antenna: (a) S_{11} with varied w, (b) S_{11} with varied t

B. Effect of the antenna depth inside human skin model

As mentioned above, the proposed planar dipole antenna is operated at dual bands and is implanted inside human tissue layers (skin, fat, muscle, and bone). In this section, the effect of the antenna depth inside the human skin model has been taken into consideration to reflection coefficient S_{11}. Fig. 5 shows this effect to S_{11} of the antenna operation in dual bands (1.5GHz and 5.8GHz). It is noted that the antenna depth inside the human 's skin arm model is greatly affected at 5.8GHz. The optimized antenna depth is selected 2mm inside the skin arm model.

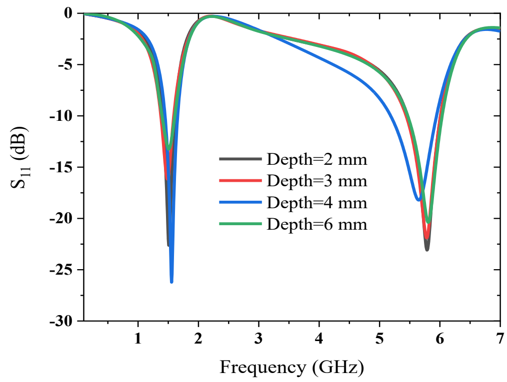

Fig. 5. Effect of the proposed antenna depth to the magnitude of the reflection coefficient S_{11}

C. Effect of the distance (d) and gold metallization thick (hc)

The variations of the distance (d) between the discrete port feeding and folded planar L-shaped of the secondary arm has been taken and effected to magnitude of the reflection coefficient S_{11}. Fig. 6 explains that the d is varied from 75μm to 125μm and it is noted at d=125μm, the performance of the proposed antenna is very poor. Therefore, the optimized value of (d) is 75μm. Also, another important parameter is affected by the performance of the antenna designed in this study. It is gold metallization thickness called (h_c) that changed from 1μm to 35μm. The effect of the thickness h_c to the reflection coefficient S_{11} at resonant frequency of 5.8GHz is more than it's affected at another resonance frequency of 1.5GHz. Fig. 7 shows the effect of the gold metal cladding h_c to magnitude of the S_{11} at dual bands. It is observed that the optimized value of the gold metal thickness has been applied is 1μm because it gives a good magnitude of S_{11} at dual resonance frequencies.

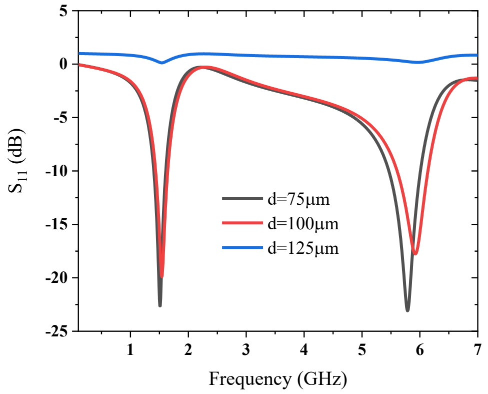

Fig. 6. Effect of the distance (d) between discrete port feeding and folded arm to magnitude S_{11}

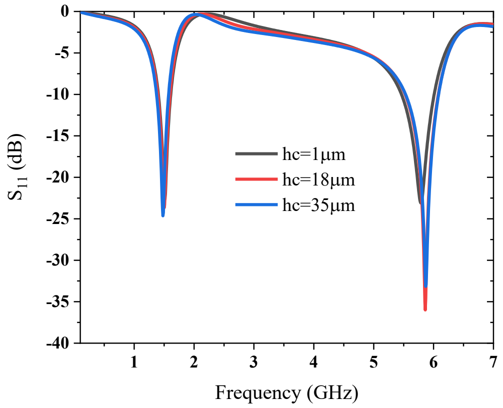

Fig. 7. Effect of the gold metallization thickness (hc) to magnitude of S11

CST microwave studio was chosen to design and simulate the antenna. Several performance parameters were taken, such as the operating resonant frequency, gain, the return loss, radiation pattern, specific absorption rate (SAR). In this section, we can divide the results in two ways. The far-field and near field simulation results.

Optimized parameter values of the planar L-shaped dipole antenna when implanted into the skin tissue of the arm model at a depth of 2mm are reported and listed in Table 1. The overall size of the proposed antenna is 2.835 mm^3 ($1\times4.5\times0.63$) mm^3. Fig. 8 shows the simulated reflection coefficient dual frequency response of the planar FDA antenna. According to reflection coefficient characteristics of the proposed implantable dipole antenna. The antenna exhibits a simulated 10-dB impedance bandwidths in a 4-layer phantom at 1.5GHz and 5.8GHz are 227MHz (1.4-1.63GHz) with S_{11} is -22.6dB and 540MHz (5.47-6.02GHz) with S_{11} is -23.1dB respectively.

The simulated far-field gain pattern when the proposed dual band antenna is implanted into the arm skin tissue is presented in Fig. 9. The maximum 3D gains and E-plane, H-plane radiation pattern are calculated to be -36.9dB, and -24.3dB for the dual resonance frequency bands 1.5GHz and 5.8GHz respectively. The electromagnetic power absorbed by the skin tissue at the proposed dual resonance frequencies is evaluated using SAR analysis. The simulated maximum 1-g and 10-g average SAR values are 426.5 and 96.8 W/kg respectively, when the proposed antenna is delivered 1W. However, according to IEEE regulations, the maximum 1-g and 10-g average SAR are both limited to values of less than 1.6 and 2 W/kg, respectively.

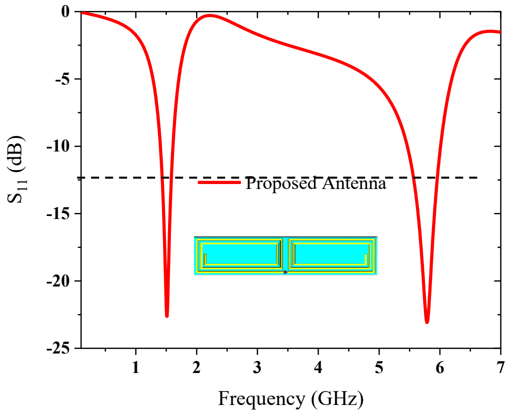

Fig. 8. Reflection coefficient S_{11} characteristics of the proposed implantable dipole antenna

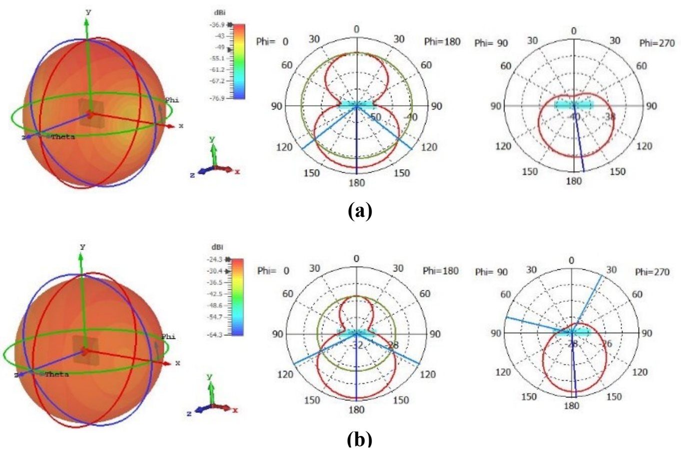

Fig. 9. Simulated far-field gain and E-plane, H-plane radiation pattern of the proposed dipole antenna implanted inside the human arm skin model at (a) 1.5GHz, (b) 5.8GHz

IV. RECTIFIER CIRCUIT DESIGN AND DISCUSSION

Due to low conversion efficiency η_{rad} and power gain of the antenna as explained and listed in table 2. To eliminate these, the voltage doubler rectifier (VDR) circuit was used which consists of two tunnel diodes D_1 and D_2 (100μm^2 QW-ASPAT) and input/output filters. The schematic diagram of the proposed rectenna circuit is shown in Fig. 10 and it comprises antenna, VDR, and load resistance (R_L). The QW-InGaAs ASPAT diodes were designed and analyzed by using SILVACO ATLAS software. The DC and RF characteristics of this diode have been simulated at zero bias voltage with different mesa size devices 16 μm^2, 36 μm^2, and 100 μm^2. In DC mode, the ASPAT (D_2) is forward biased during the negative half cycle, the (C_2) is charged to peak amplitude voltage received. For the positive cycle, the D_1 is ON, then the C_2 will be holding double amplitude. The DC simulation of the QW-InGaAs ASPATs is shown in Fig. 11.

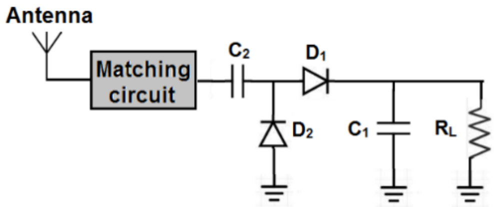

Fig. 10. The schematic of the rectenna circuit design

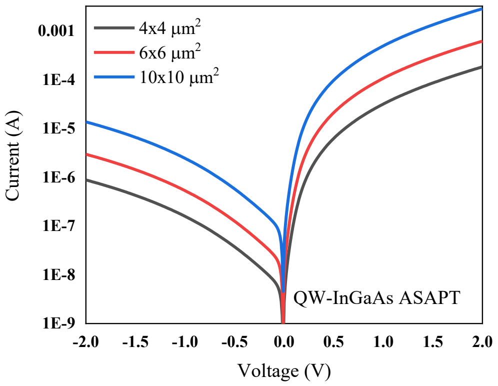

Fig. 11. DC characteristics of the QW ASPAT tunnel diode

The key parameters of the 10x10µm^2 QW-ASPAT device are curvature coefficient (K_v), junction resistance (R_j), junction capacitance (C_j) and series resistance (R_s). These parameters extracted from the both DC and RF characteristics are 33V^{-1}, 206kΩ, 65.6fF, and 53Ω respectively.

V. RECTENNA CIRCUIT DESIGN AND ANALYSIS

As mentioned above, the proposed antenna is implanted inside human 's arm and can be used for low power implantable medical devices. The overall volume size of the compact proposed FDA antenna is 2.84mm^3. The QW-ASPAT device with 10MLs thin barrier thickness has been used as a rectifier diode in the rectifying circuit and integrated with the antenna. The matching between the input impedance of the antenna and rectifying circuit can be achieved, when the real part of the both devices are similar and the imaginary part is cancelled at a specific frequency. Fig. 12 describes the S_{11} parameter for the antenna designed in CST and circuit model in ADS library. Fig. 13 shows the equivalent circuit model of the compact rectenna circuit which integrated the antenna with QW-ASPAT rectifier diode. The 1×4.5mm^2 antenna impedance (Z_{Ant}) obtained previously are (58+j*2) Ω and (57+j*2.4) Ω for dual band respectively and listed in table 2. The input impedance ($Z_{in\ ASPAT}$) of this diode is dependent on resonant frequency, R_s, R_j, and C_j. The $Z_{in\ ASPAT}$ can be calculated mathematically by expression in Eq. (2).

$$Z_{in(QW-ASAPT)} = R_s + \frac{1}{1+w^2C_j^2R_j^2} - j\frac{wC_jR_j}{1+w^2C_j^2R_j^2} \qquad \text{.................} (2)$$

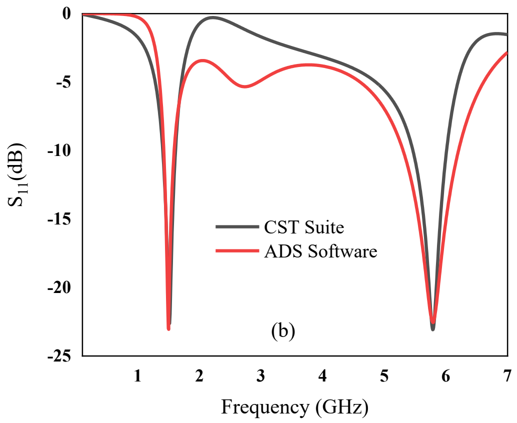

Fig. 12. The S_{11} parameter of the antenna by both software ADS and CST

The impedance $Z_{in(QW-ASAPT)}$ of the 100µm^2 size device are (65-j*1620)Ω and (53-j*418)Ω for dual band 1.5GHz and 5.8GHz respectively. In order to achieve perfect matching between QW-ASPAT diode and antenna, we must calculate the input impedance of the VDR circuit $Z_{in(VDR)}$ that contains the QW-ASPAT diodes (D_1 and D_2). The $Z_{in(VDR)}$ for proposed dual bands are (56-j*915)Ω and (58-j*236)Ω respectively at input power of the antenna is 10dBm. It observed from results that the real part impedance of the antenna and VDR circuit are matched compared with different imaginary parts. The reactance part can be cancelled by adding an input matching network which is constructed on the ADS library. Fig. 14 shows the simulated return loss at dual bands of the matching response between the proposed planar 4.5 L-section 1×4.5mm^2 dipole antenna and the QW-ASPAT diodes. The rectenna circuit exhibited reasonable matching performance at an input RF power of 10dBm as well.

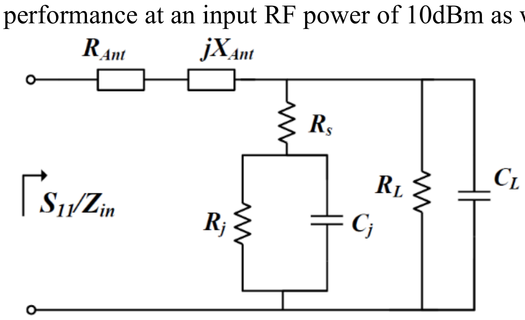

Fig. 13. Implantable rectenna equivalent circuit model

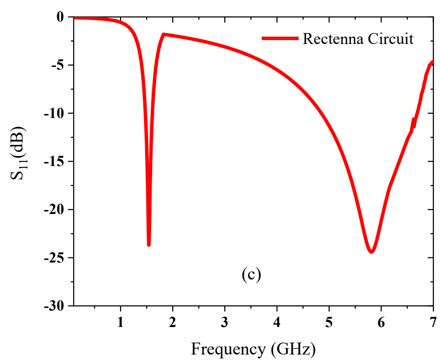

Fig. 14. Return loss of the implantable proposed rectenna circuit model

The DC voltage component at the output termination is acquired by the R_L and C_L. Of course, a higher R_L results in a higher output voltage. The DC output voltage which is provided from the implantable rectenna circuit is used to wireless power transfer to implantable medical devices inside the human arm model. Fig. 15 shows the DC-output voltage (V_{out}) and power (P_{out}) of the rectenna model by using single and double stage of the VDR circuit at optimum R_L of 10kΩ.

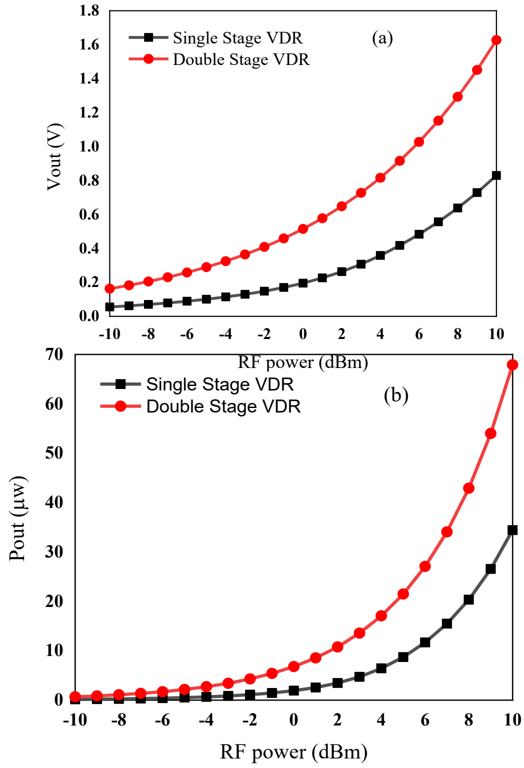

Fig. 15. The DC output voltage and power of the rectenna circuit with single and double stage VDR circuit at frequency of 5.8GHz for (a), and (b) respectively

VI. CONCLUSIONS

A dual band miniaturized fully integrated rectenna circuit for implantable medical devices has been designed and analyzed inside a skin human 's arm model for WMTS (1.5GHz) and ISM (5.8GHz) bands operation. The proposed L-shaped planar dipole antenna (FDA) exhibits a simulated 10-dB impedance bandwidth at 1.5 GHz and 5.8GHz are 227MHz (1.4-1.63GHz) with S_{11} is -22.6dB and 540MHz (5.47-6.02 GHz) with S_{11} is -23.1dB, whereas gains are -36.9dBi, and -24.3dBi, respectively. The overall physical volume of the FDA is 2.84 mm^3 which occupies the smallest volume of all, it presents one of the best combinations of size. Additionally, the antenna produces a far-field radiation pattern that is almost omnidirectional. The tunnel 100μm^2 QW InGaAs ASPAT diode has been designed by SILVACO software and it was used as a rectifying circuit to convert RF power to DC voltage for charging medical devices. The voltage doubler rectifier (VDR) circuit was used as a single and double stage, the DC output voltage and power of the rectenna for double stage rectifiers are twice that produced by the single stage at the input RF power of 10dBm. We can observe that the effective folded approach used within the dipole structure improves the miniaturization of the planar antenna while also offering equivalent performance characteristics to recently implanted antennas reported in the literature review by table III.

TABLE III
PERFORMANCE COMPARISON OF LITERATURES REVIEW WITH RESPECT PROPOSED ANTENNA CHARACTERISTICS

Ref. Year	Proposed Antenna Structures	Resonant frequency [GHz]	Gain [dBi]	B.W [MHz]	Dimension [mm]
[20] 2018	Miniaturized DGS serpentine.	ISM 2.4-2.48	-11	762	44×6×0.78
[21] 2020	Microstrip patch with spiral split rings.	0.915	-38.8	68.3	14×14×3
		ISM 0.433	-38.1		
[22] 2021	Compact triple-band implant spiral structure	0.402	-23	93	π×(11.2)²×0.5
		WMTS 1.4	-20.5	202	
		ISM 2.45	-19	444	
[23] 2018	Compact Meander structure	0.401-0.406	---	133	30.5×21.02×1
[24] 2021	Meandered triple-band PIFA structure	0.402	−43.6	90	11×20.5×1.8
		0.902	−25.8	---	
		2.4	−20.1	190	
[25] 2020	Dual-band fractal geometry antenna	MICS 0.4	−28.1	22.8	9.5× 9.5×0.6
		ISM 2.45	−31.3	13.1	
[26] 2018	Flower-shape dual band patch	0.928	-28.44	184.1	7×7.2×0.2
		ISM 2.45	-25.65	219.7	
[27] 2021	Miniaturized circular maze shaped antenna	ISM 2.42–2.48	-23	286	7×7×0.1
[28] 2019	Novel meander integrated E-shaped.	ISM 2.2-2.5	3.78	370	60×60×4.6
[29] 2020	Compact hexagonal shaped microstrip patch	ISM 2.45	6.14	230	100×100×1.6
[30] 2020	Compact pentagon-shaped microstrip patch	ISM 2.45	8.02	240	100×100×1.6
[34] 2021	Implantable circular-shaped meandered PIFA.	ISM 2.43	-9.49	61.24	π×(7.5)²×1.5
[35] 2021	implant Multilayer PIFA meandering	MICS 0.402-0.405	-21	20	12×7×3.94
[36] 2021	Rectangular micro-strip patch loaded with F shaped slot.	ISM 2.4–2.48	12	300	13×16×1
[37] 2019	Multilayer PIFA Archimedean spiral	0.403	-38	35	π×(5)²×0.76
		ISM 0.435	-40.1	50	
[38] 2021	Circular dual-band implantable antenna	0.400	−33.1	153	π×(10)²×2.5
		ISM 2.45	−14	422	
[39] 2020	Dual-band implant PIFA antenna	ISM 2.45	3.77	136.3	10×9.5×1.5
		ISM 5.2	2.53	73	
[40] 2018	Microstrip patch with a short pin	ISM 2.4	-20.8	350	11×11×0.6
[41] 2019	Circular shaped fractal-patch with DGS structure	2.45	-20.8	2570	40×40×1.6
		4.22	-35.1	---	
This Work	Implantable planar L-Shaped FDA antenna	WMTS 1.5	-36.9	227	4.5×1×0.63
		ISM 5.8	-24.3	540	

ACKNOWLEDGEMENTS

The authors are very grateful to the University of Mosul/College of Engineering for their provided facilities, which helped to improve the quality of this work.

REFERENCES

[1] M. Kumar, "Social, economic, and environmental impacts of renewable energy resources," Wind Solar Hybrid Renewable Energy System, vol. 1, 2020.

[2] H. Liu, H. Fu, L. Sun, C. Lee, and E. M. Yeatman, "Hybrid energy harvesting technology: From materials, structural design, system integration to applications," Renewable and sustainable energy reviews, vol. 137, p. 110473, 2020. https://doi.org/10.1016/j.rser.2020.110473

[3] P. Jiao, W. Borchani, H. Hasni, and N. Lajnef, "Enhancement of quasi-static strain energy harvesters using non-uniform cross-section post-buckled beams," Smart Materials and Structures, vol. 26, no. 8, p. 085045, 2017. https://doi.org/10.1088/1361-665X/aa746e

[4] A. Mohammadnia, A. Rezania, B. M. Ziapour, F. Sedaghati, and L. Rosendahl, "Hybrid energy harvesting system to maximize power generation from solar energy," Energy Conversion and Management, vol. 205, p. 112352, 2020. https://doi.org/10.1016/j.enconman.2019.112352

[5] Q. Wen, X. He, Z. Lu, R. Streiter, and T. Otto, "A comprehensive review of miniatured wind energy harvesters," Nano Materials Science, vol. 3, no. 2, pp. 170–185, 2021. https://doi.org/10.1016/j.nanoms.2021.04.001

[6] A. Nozariasbmarz et al., "Review of wearable thermoelectric energy harvesting: From body temperature to electronic systems," Applied Energy, vol. 258, p. 114069, 2020.

[7] R. Subbaramaiah, S. A. Al-Jufout, A. Ahmed, and M. M. Mozumdar, "Design of vibration-sourced piezoelectric harvester for battery-powered smart road sensor systems," IEEE Sensors Journal, vol. 20, no. 23, pp. 13940–13949, 2020. https://doi.org/10.1109/JSEN.2020.300048

[8] S. Roy, J.-J. Tiang, M. B. Roslee, M. Ahmed, A. Z. Kouzani, and M. Mahmud, "Design of a Highly Efficient Wideband Multi-Frequency Ambient RF Energy Harvester," Sensors, vol. 22, no. 2, p. 424, 2022. https://doi.org/10.3390/s22020424

[9] S. A. A. Shah and H. Yoo, "Radiative near-field wireless power transfer to scalp-implantable biotelemetric device," IEEE Transactions on Microwave Theory and Techniques, vol. 68, no. 7, pp. 2944–2953, 2020. https://doi.org/10.1109/TMTT.2020.2985356

[10] M. T. Bevacqua, G. G. Bellizzi, and M. Merenda, "An efficient far-field wireless power transfer via field intensity shaping techniques," Electronics, vol. 10, no. 14, p. 1609, 2021. https://doi.org/10.3390/electronics10141609

[11] A. M. Sabaawi and O. A. Al-Ani, "Solar Rectennas: Analysis and Design," in Recent Wireless Power Transfer Technologies, IntechOpen, 2019. https://doi.org/10.5772/intechopen.89216

[12] M. Al-Hasan, P. R. Sura, A. Iqbal, J. J. Tiang, I. B. Mabrouk, and M. Nedil, "Low-profile dual-band implantable antenna for compact implantable biomedical devices," AEU-International Journal of Electronics and Communications, vol. 138, p. 153896, 2021. https://doi.org/10.1016/j.aeue.2021.153896

[13] N. Marriwala, "Energy Harvesting System Design and Optimization Using High Bandwidth Rectenna for Wireless Sensor Networks," Wireless Personal Communications, vol. 122, no. 1, pp. 669–684, 2022. https://doi.org/10.1007/s11277-021-08918-x

[14] P. Sharma and A. K. Singh, "A Compact Antenna Design with High Gain for Wireless Energy Harvesting," in Computational Methodologies for Electrical and Electronics Engineers, IGI Global, 2021, pp. 244–253. https://doi.org/10.4018/978-1-7998-3327-7.ch019

[15] N. Saranya and T. Kesavamurthy, "Review on next generation wireless power transmission technology for implantable biomedical devices," International Journal of Biomedical Engineering and Technology, vol. 35, no. 3, pp. 207–222, 2021. https://doi.org/10.1504/IJBET.2021.113730

[16] A. N. Khan, Y. Cha, H. Giddens, and Y. Hao, "Recent advances in organ specific wireless bioelectronic devices: Perspective on biotelemetry and power transfer using antenna systems," Engineering, 2022. https://doi.org/10.1016/j.eng.2021.10.019

[17] M. N. Hasan, S. Sahlan, K. Osman, and M. S. Mohamed Ali, "Energy harvesters for wearable electronics and biomedical devices," Advanced Materials Technologies, vol. 6, no. 3, p. 2000771, 2021. https://doi.org/10.1002/admt.202000771

[18] V. Sadadiwala, K. Mahindroo, V. Singh, P. Bansal, and S. Singhal, "Human Body Monitoring Wearable Antenna," in Optical and Wireless Technologies, Springer, 2022, pp. 151–161. DOI:10.1007/978-981-16-2818-4_16

[19] Y. Feng, Z. Li, L. Qi, W. Shen, and G. Li, "A compact and miniaturized implantable antenna for ISM band in wireless cardiac pacemaker system," Scientific Reports, vol. 12, no. 1, pp. 1–11, 2022. https://doi.org/10.1038/s41598-021-04404-3

[20] S. Sukhija, R. K. Sarin, and N. Kashyap, "Design of compact wideband serpentine patch antenna for ingestible endoscopic applications," Progress In Electromagnetics Research M, vol. 66, pp. 53–63, 2018.

[21] A. Rula, "Patch antenna based on spiral split rings for bone implants," Przegląd Elektrotechniczny, vol. 96, 2020.

[22] T.-A. Le Trong, S. I. H. Shah, G. Shin, S. M. Radha, and I.-J. Yoon, "A compact triple-band antenna with a broadside radiation characteristic for head-implantable wireless communications," IEEE Antennas and Wireless Propagation Letters, vol. 20, no. 6, pp. 958–962, 2021. https://doi.org/10.1109/LAWP.2021.3068170

[23] N. Samsuri, M. Rahim, F. Seman, and M. Inam, "Compact meander line telemetry antenna for implantable pacemaker applications," Indones. J. Electr. Eng. Comput. Sci, vol. 10, pp. 883–889, 2018. https://doi.org/10.11591/ijeecs.v10.i3.pp883-889

[24] N. Pournoori, L. Sydänheimo, Y. Rahmat-Samii, L. Ukkonen, and T. Björninen, "Small Triple-Band Meandered PIFA for Brain-Implantable Biotelemetric Systems: Development and Testing in a Liquid Phantom," International Journal of Antennas and Propagation, vol. 2021, 2021. https://doi.org/10.1155/2021/6035169

[25] Y. Fan, H. Liu, X. Liu, Y. Cao, Z. Li, and M. M. Tentzeris, "Novel coated differentially fed dual-band fractal antenna for implantable medical devices," IET Microwaves, Antennas & Propagation, vol. 14, no. 2, pp. 199–208, 2020. https://doi.org/10.1049/iet-map.2018.6171

[26] F. Faisal and H. Yoo, "A miniaturized novel-shape dual-band antenna for implantable applications," IEEE Transactions on Antennas and Propagation, vol. 67, no. 2, pp. 774–783, 2018. https://doi.org/10.1109/TAP.2018.2880046

[27] C. Gayathri and S. Venkatanarayanan, "A miniaturized circular maze shaped antenna for implantable health care applications," Journal of Ambient Intelligence and Humanized Computing, vol. 12, no. 5, pp. 4757–4763, 2021. https://doi.org/10.1007/s12652-020-01884-5

[28] K. Çelik and E. Kurt, "A novel meander line integrated E-shaped rectenna for energy harvesting applications," International Journal of RF and Microwave Computer-Aided Engineering, vol. 29, no. 1, p. e21627, 2019. https://doi.org/10.1002/mmce.21627

[29] D. Surender, T. Khan, and F. A. Talukdar, "A hexagonal-shaped microstrip patch antenna with notch included partial ground plane for 2.45 GHz Wi-Fi band RF energy harvesting applications," 2020, pp. 966–969. https://doi.org/10.1080/09205071.2021.1970030

[30] D. Surender, T. Khan, and F. A. Talukdar, "A pentagon-shaped microstrip patch antenna with slotted ground plane for RF energy harvesting," 2020, pp. 1–4.

[31] S. H. Hussein, S. W. Luhabi, M. T. Yaseen, and M. Jasim, "Study and design of class f power amplifier for mobile applications," J. Eng. Sci. Technol, vol. 16, no. 5, pp. 3822–3834, 2021.

[32] S. G. Muttlak, M. Sadeghi, K. Ian, and M. Missous, "Miniaturized Folded Antenna with Improved Matching Characteristic for mm-wave Detections," 2021, pp. 1–3. https://doi.org/10.1109/UCMMT53364.2021.9569948

[33] S. H. Hussein, "Design and Simulation of a High Performance CMOS Voltage Doublers using Charge Reuse Technique," Journal of Engineering Science and Technology, vol. 12, no. 12, pp. 3344–3357, 2017. ISBN: 1823-4690

[34] M. Samad, M. M. Rahman, and S. Shamim, "Design of a Miniaturized Implantable PIFA with DGS for the Investigation of Uterus Fibroids," 2021.
https://doi.org/10.19044/esj.2021.v17n37p211

[35] R. B. Khadase, A. Nandgaonkar, B. Iyer, and A. Wagh, "Multilayered Implantable Antenna Biosensor for Continuous Glucose Monitoring: Design and Analysis," Progress In Electromagnetics Research C, vol. 114, pp. 173–185, 2021. https://doi.org/10.2528/PIERC21052203

[36] T. Sathiyapriya, V. Gurunathan, and J. Dhanasekar, "Design of an implantable antenna for biomedical applications," 2021.

[37] R. Kumar, L. S. Solanki, and S. Singh, "Miniature Archimedean spiral PIFA antennas for biomedical implantable devices," 2019, pp. 162–167. https://doi.org/10.1109/SPIN.2019.8711600

[38] N. Ganeshwaran, J. K. Jeyaprakash, M. G. N. Alsath, and V. Sathyanarayanan, "Design of a dual-band circular implantable antenna for biomedical applications," IEEE Antennas and Wireless Propagation Letters, vol. 19, no. 1, pp. 119–123, 2019.
https://doi.org/10.1109/LAWP.2019.2955140

[39] M. M. Khan and T. Hossain, "Compact Planar Inverted F Antenna (PIFA) for Smart Wireless Body Sensors Networks," 2020, vol. 2, no. 1, p. 63. https://doi.org/10.3390/ecsa-7-08253

[40] Z.-J. Yang and S. Xiao, "A wideband implantable antenna for 2.4 GHz ISM band biomedical application," 2018, pp. 1–3.